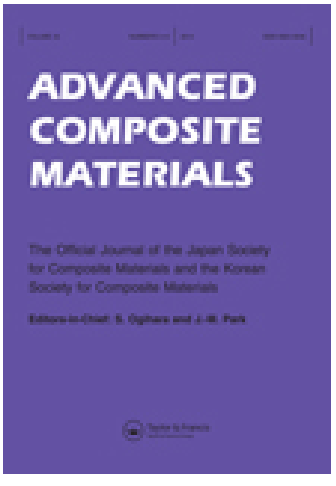

Advanced Composite Materials
Publication details, including instructions for authors and subscription information:
http://www.tandfonline.com/loi/tacm20

Applicability of micro-macro decoupling scheme to two-scale analysis of fiber-reinforced plastics

Kenjiro Terada[a], Norio Hirayama[b], Koji Yamamoto[c], Junji Kato[d], Takashi Kyoya[d], Seishiro Matsubara[d], Yusuke Arakawa[d], Yuta Ueno[b] & Naohiro Miyanaga[b]

[a] International Research Institute of Disaster Science, Tohoku University, Aza-Aoba 6-6-11-1302, Aramaki, Aoba-ku, Sendai, Miyagi 980-8579, Japan

[b] Fukushima Research Center, Nitto Boseki Co., Ltd., 20 Sakura Ipponsugi, Fukushima 960-2154, Japan

[c] Cybernet Systems Co. Ltd., Kanda-neirikabe-cho, Chiyoda-ku, Tokyo 101-0022, Japan

[d] Department of Civil Engineering, Tohoku University, Aza-Aoba 06, Aramaki, Aoba-ku, Sendai, Miyagi 980-8579, Japan

Published online: 12 May 2014.

To cite this article: Kenjiro Terada, Norio Hirayama, Koji Yamamoto, Junji Kato, Takashi Kyoya, Seishiro Matsubara, Yusuke Arakawa, Yuta Ueno & Naohiro Miyanaga (2014) Applicability of micro-macro decoupling scheme to two-scale analysis of fiber-reinforced plastics, Advanced Composite Materials, 23:5-6, 421-450, DOI: 10.1080/09243046.2014.915098

To link to this article: http://dx.doi.org/10.1080/09243046.2014.915098

Advanced Composite Materials, 2014
Vol. 23, Nos. 5–6, 421–450, http://dx.doi.org/10.1080/09243046.2014.915098

Applicability of micro–macro decoupling scheme to two-scale analysis of fiber-reinforced plastics

Kenjiro Terada[a]*, Norio Hirayama[b], Koji Yamamoto[c], Junji Kato[d], Takashi Kyoya[d], Seishiro Matsubara[d], Yusuke Arakawa[d], Yuta Ueno[b] and Naohiro Miyanaga[b]

[a]*International Research Institute of Disaster Science, Tohoku University, Aza-Aoba 6-6-11-1302, Aramaki, Aoba-ku, Sendai, Miyagi 980-8579, Japan;* [b]*Fukushima Research Center, Nitto Boseki Co., Ltd., 20 Sakura Ipponsugi, Fukushima 960-2154, Japan;* [c]*Cybernet Systems Co. Ltd., Kanda-neirikabe-cho, Chiyoda-ku, Tokyo 101-0022, Japan;* [d]*Department of Civil Engineering, Tohoku University, Aza-Aoba 06, Aramaki, Aoba-ku, Sendai, Miyagi 980-8579, Japan*

(*Received 30 December 2013; accepted 24 March 2014*)

The numerical study is made to demonstrate the applicability of the *method of decoupling multi-scale analysis* to the micro–macro evaluation of the mechanical behavior of fiber-reinforced plastics (FRP) that exhibits inelastic deformations and internal damage of the matrix material. During the course of this demonstration, it is confirmed that the reliability of the decoupling method can be guaranteed if the macroscopic constitutive model is introduced so as to inherit the microscopic material behavior. To this end, with reference to the results of the numerical material testing on the periodic microstructures of FRP, we propose an anisotropic elastoplastic-creep-damage combined constitutive model to represent the macroscopic material behavior and illustrate the characteristics of the inelastic deformations that resemble the material behavior assumed for plastics at micro-scale. With the identified macroscopic material parameters, the macroscopic structural analysis, which is followed by the localization analysis consistently, can be an actual proof of the utility value of the decoupling method in practice.

Keywords: decoupling multi-scale analysis; FRP; homogenization; elastoplasticity; creep; damage

1. Introduction

On recorded history of fiber-reinforced plastic (FRP), much ink has been spent on the derivation of analytical or approximate expressions for its effective or overall material properties, and the manifold achievement led to the field of study called *micromechanics* and *mechanics of composite materials*, often along with representative volume elements (RVE), over which the averaging is performed; see e.g. [1–4] for early developments and [5–10] as standard textbooks. Although these theoretical developments have successfully enabled us to understand the roles that individual phases play in the overall macroscopic behavior of FRP, it has been recognized over the past few decades that computational approaches are more capable of providing efficiency and flexibility in designing composite materials. In fact, numerical simulation techniques such as the finite element method (FEM) are indispensable nowadays to meet advanced demands for further strengthening of FRP with low cost in engineering practice; see e.g. textbooks

*Corresponding author. Email: tei@irides.tohoku.ac.jp

[11–15] and references therein. However, reflecting the geometrical characteristics of constituents at the micro-scale, the macroscopic mechanical behavior of FRP is often too complicated to characterize, especially when FRP undergoes non-linear and/or inelastic material behavior. This complexity sometimes makes it difficult for us to perform reliable numerical simulations and thus has provoked a great deal of controversy.

In this context, the method of multi-scale analysis based on the homogenization theory [16–18] has been recognized as a rigorous methodology for characterizing the macro-scale mechanical behavior of heterogeneous media with periodic microstructures (unit cells). Thanks to its rigorous mathematical background,[19] this computational homogenization approach for FRP enables us not only to reflect the geometrical features at micro-scale such as layout of fibers, shape, and size of constituents in the characterization of macroscopic material properties (homogenization process), but also to reproduce the true micromechanical responses towards the actual external and macroscopic deformations (localization process). Since the capabilities of these micro-to-macro and macro-to-macro transitions are favorable even for non-linear problems, the homogenization-based multi-scale analysis methods have successfully been applied even to problems involving inelastic material behavior such as damage in FRPs; see e.g. [20–26].

Nonetheless, its applicability to non-linear/inelastic problems is still limited in practice, especially when we are concerned with the interaction between the mechanical responses of micro- and macro-scale structures of FRPs, which can be obtained as a set of solutions of the so-called two-scale boundary value problem (BVP) derived for a non-linear homogenization problem. This limited applicability is due to the fact that the macroscopic constitutive equation in the two-scale BVP is an implicit function of the solutions of the micro-scale BVP or, in other words, the micro-scale BVP only indirectly represents the macroscopic material response. That is, it is not until the micro-scale equilibrated stress is determined that the macroscopic stress can be calculated with the following averaging relation:

$$\tilde{\boldsymbol{A}} = \frac{1}{|V|}\int_V \boldsymbol{A}\,dV, \tag{1}$$

which defines the volume average $\tilde{\boldsymbol{A}}$ of a second-order tensor $\boldsymbol{A}$ over the unit cell's domain with $|V|$ being the volume of domain V. Therefore, if the coupling analysis is performed to solve the two-scale BVP by the FEM, then the micro-scale BVP must be associated with an integration point located in a macro-scale finite element (FE) model and solved for the micro-scale equilibrated stress to evaluate the macro-scale stress by the averaging relation (1), which must satisfy the macro-scale BVP at the same time. In particular, when an implicit and incremental solution method with a Newton–Raphson-type iterative procedure is employed to solve the two-scale BVP, the micro-scale BVP is to be solved in every iteration to attain the macro-scale equilibrium state at every loading step. Needless to say, the micro-scale BVP is also non-linear and therefore requires the iterative method. This type of solution scheme to solve the two-scale BVP is referred to as the micro–macro (or global–local) coupling scheme and is typified in [27–33].

The micro–macro coupling scheme is robust and promising in the sense that various types of macroscopic material behaviors can be captured without knowing their explicit functional forms of material models if the unit cell is eligible for a RVE. In fact, this seems to be the only way to evaluate the non-linear macroscopic material response of a

heterogeneous medium when the analytical expression of its macroscopic constitutive relation is hard to formulate; see e.g. Refs [34,35]. However, the nature of the method means that it requires a significant amount of computational cost. In fact, the model size of the macro-scale BVP raises the number of micro-scale BVPs to the second power, since each macro-scale integration point is associated with its own micro-scale BVP. Although other remedies [27,36,37] and parallel algorithms [38] can reduce the cost to some extent, we are bound to say that the coupling scheme is all but useless in most practical applications.

Therefore, the decoupling of micro- and macro-scale BVPs is indispensable for applying the two-scale approach based on the homogenization theory to various non-linear problems encountered in practice. This motivates us to take an alternative approach, called the micro–macro decoupling scheme.[39,40] The decoupling scheme strongly relies on the method of *numerical material testing* (NMT), which corresponds to the homogenization process for the unit cells, just like the computational homogenization method for linear problems. To be more specific, assuming the concrete functional form of the macro-scopic constitutive model, we conduct a series of NMTs on the *numerical specimen*, i.e. the unit cell's FE model, to obtain the non-linear macro-scale material behavior. By means of the 'measured' data in the NMTs, the material parameters in the assumed constitutive model are determined with an appropriate method of parameter identification. Once the macro-scale material behavior is successfully fitted with the identified parameters, the macro-scale analysis can be performed, and, as may be necessary, the macro-scale deformation history at any point in the macro-structure can be applied to the unit cell to evaluate the actual micro-scale response.

The precondition of the decoupling scheme is that we are able to pick up a constitutive model to properly characterize the macroscopic material behavior that would be obtained from the numerical analysis on the micro-scale BVP. It is noted that, from a practical point of view, approximated constitutive models allow alternatives, since there might not be a rigorous model available depending on the type of composite materials. Once the functional form of an appropriate macroscopic constitutive equation is assumed, several micro-scale numerical analyses are performed on the unit cell to obtain its material parameters. The set of micro-scale analyses for this purpose can be referred to as the NMT, an essential process of the micro–macro decoupling scheme.[39,40] The concrete procedure of the method is described as follows:

(i) An appropriate constitutive model relevant for the macroscopic material behavior under consideration is assumed.
(ii) A series of the NMTs is conducted on a unit cell model (FE mesh), which is regarded as a 'numerical specimen,' to obtain the homogenized or macroscopic material behavior. Note that the loading patterns here hinge on the selected constitutive model.
(iii) Material parameters of the assumed constitutive model are identified by means of the 'empirical' data obtained from the NMTs and an appropriate curve-fitting scheme.
(iv) FE analyses are carried out to solve the macro-scale BVP using the assumed constitutive model with identified material parameters.
(v) If necessary, after extracting the time series of macroscopic deformation history from the macroscopic analysis result and applying it as a series of boundary conditions, the localization analyses are performed to evaluate what

has actually been happening inside the unit cell during the macroscopic deformation process.

Then, the objective of this study is set forth to demonstrate the applicability of the decoupling multi-scale analysis method to a variety of inelastic material behavior exhibited by FRP. The key angle in this context is that the macroscopic material behavior must inherit the microscopic one employed for NMT. Since the material models used in unit cells are supposed to be given in the computational homogenization method, the homogenized or macroscopic material model to be assumed in step (i) is expected to fully or partially inherit the micro-scale material characteristics. For example, if the unit cell model of unidirectional FRP is assumed to be composed of *isotropic* hyperelastic materials, the corresponding macroscopic material behavior can be *transversely isotropic* hyperelastic. Likewise, if the constituents are elastoplastic materials, the macroscopic constitutive model should be within the scope of anisotropic plasticity. Even though micro-scale cracking is taken into account as in [35], the corresponding macroscopic material behavior may be represented by the anisotropic damage model approximately. To accomplish the objective from this viewpoint, we set up a sample problem for unidirectional CFRP whose matrix phase exhibits rate-dependent and rate-independent inelastic material behaviors with internal damage and carry out a two-scale de-coupled analysis to confirm the above-mentioned anticipation. During the course of the confirmation, we propose an anisotropic elastoplastic-creep-damage combined constitutive model to represent the macroscopic material behavior and illustrate the characteristics of the inelastic deformations that resemble the material behavior assumed for plastics at micro-scale. Then, the analogies between the micro- and macroscopic constitutive models are illustrated in terms of functional characteristics.

2. Material model for resin in CFRP

In this section, the inelastic material behavior of resin in CFRP is characterized with reference to the data obtained in the loading–unloading tests. On the other hand, the carbon fibers are assumed to be linearly elastic and isotropic for the sake of simplicity. After the test results on the polycarbonate resin are studied, a set of constitutive equations is introduced to be used for the material model of the resin.

2.1. Uniaxial loading–unloading test for polycarbonate resin

Two sets of uniaxial loading–unloading tests were conducted on standard testing specimens of polycarbonate resin under deformation rate control at room temperature (20 °C). Figure 1 shows the obtained nominal stress–strain curves, which were transformed from the corresponding load–displacement curves. Here, two deformation rates (0.001/s and 0.0001/s) were employed to control the elongation of the specimens, which were subjected to loading until the strain reaches about 5 % and unloading until the reaction force becomes zero. From these curves, we can itemize the following five features of the material behavior of the polycarbonate resin:

(a) Residual (or permanent) deformations are observed.
(b) Dependency of the apparent stiffness depends on the strain rates (the faster the strain rate, the higher the apparent stiffness).

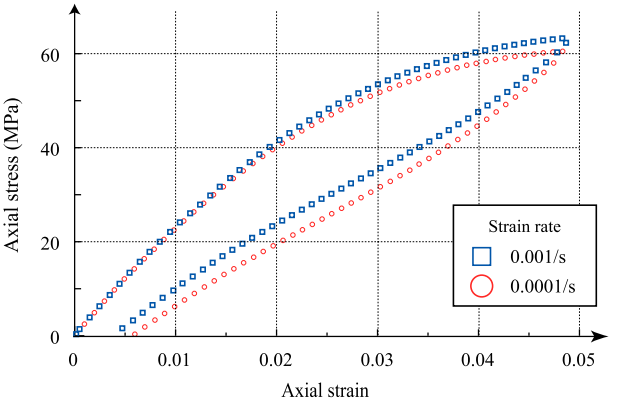

Figure 1. Stress vs. strain curves obtained from loading–unloading tests for polycarbonate resin.

(c) Dependency of the amount of residual deformations depends on the strain rates (the faster the strain rate, the smaller the residual deformation).
(d) Reduction of the elastic modulus accompanying the progress of deformations (the elastic modulus during the unloading regime is smaller than that of the loading regime).
(e) Non-linearity of the unloading curve.

Here, it is reasonable to regard the residual strains pointed out in (a) as plastic or creep strains, but difficult to distinguish rate-independent or rate-dependent ones only from features (b) and (c). Also, the reduction of apparent stiffness during the loading regime is caused not only by inelastic (plastic or creep) deformations, but also by the internal damage. In fact, feature (d) described for the unloading regime implies the reduction of elastic modulus even during the loading regime. Finally, though item (e) might be one of the essential features of the resin, it is enough to incorporate features (a)–(d) into the decoupling method in view of the purpose of this study.

In summary, the resin under consideration possibly exhibits both the rate-dependent material behavior accompanying creep strains and the rate-independent behavior accompanying plastic strains. At the same time, the elastic modulus can be reduced due to the material damage at molecule level, implying that the stress transmission ability is decreased.

Based on the above discussions, in this study, we employ an elastoplastic-creep-damage combined model to represent the material behavior of the polycarbonate resin in CFRP. The rate-dependent and rate-independent permanent strains are, respectively, represented with standard creep and elastoplasticity constitutive models, while the reduction of the elastic modulus is typified in classical continuum damage theory. The model presented in this study is not probably new, but to the best of the authors' knowledge has not been used to characterize the material behavior of resin in CFRP especially within the framework of homogenization-based multi-scale method.

2.2. Isotropic elastoplastic-creep-damage combined model

An isotropic elastoplastic-creep-damage combined model is introduced for the material behavior of the polycarbonate resin, whose uniaxial responses are studied above. A set of constitutive equations for each of elastic, plastic, creep, and damage models is presented in order, and then unified to form the combined model. Although a considerable number of studies have been made on the constitutive equations for resin-type materials within the framework of finite strain–strain theory,[41] the infinitesimal strain theory is enough for the model employed here, since we are concerned with the analogy between the micro- and macroscopic material models in this study. In fact, the deformations observed in the above uniaxial tests were not severely large.

2.2.1. Additive decomposition of inelastic strain

We employ the following additive decomposition of the total strain $\boldsymbol{\varepsilon}$:

$$\boldsymbol{\varepsilon} = \boldsymbol{\varepsilon}^{\mathrm{e}} + \boldsymbol{\varepsilon}^{\mathrm{p}} + \boldsymbol{\varepsilon}^{\mathrm{c}} = \boldsymbol{\varepsilon}^{\mathrm{e}} + (\boldsymbol{\varepsilon}^{\mathrm{p}}_{\mathrm{vol}} + \boldsymbol{e}^{\mathrm{p}}) + (\boldsymbol{\varepsilon}^{\mathrm{c}}_{\mathrm{vol}} + \boldsymbol{e}^{\mathrm{c}}) \tag{2}$$

where $\boldsymbol{\varepsilon}^{\mathrm{e}}$, $\boldsymbol{\varepsilon}^{\mathrm{p}}$, and $\boldsymbol{\varepsilon}^{\mathrm{c}}$ are elastic, plastic, and creep strains, respectively. Here, $\boldsymbol{\varepsilon}^{\mathrm{p}}_{\mathrm{vol}}$ and $\boldsymbol{e}^{\mathrm{p}}$ are volumetric and deviatoric parts of the plastic strain, respectively, and $\boldsymbol{\varepsilon}^{\mathrm{c}}_{\mathrm{vol}}$ and $\boldsymbol{e}^{\mathrm{c}}$ are those of the creep strain. Since the incompressibility of the plastic strains can often be assumed for standard resin materials, we employ the assumption so that $\boldsymbol{\varepsilon}^{\mathrm{p}}_{\mathrm{vol}} \approx 0$ and $\boldsymbol{\varepsilon}^{\mathrm{c}}_{\mathrm{vol}} \approx 0$.

2.2.2. Constitutive equations for elastic materials

The elastic behavior is assumed to be isotropic so that the following generalized Hooke's law can be employed:

$$\boldsymbol{\sigma} = \mathbb{C}^{\mathrm{e}} : \boldsymbol{\varepsilon}^{\mathrm{e}} = (\kappa \mathbf{1} \otimes \mathbf{1} + 2\mu \boldsymbol{I}^{\mathrm{dev}}) : \boldsymbol{\varepsilon}^{\mathrm{e}} = \kappa \epsilon^{\mathrm{e}}_{\mathrm{v}} \mathbf{1} + 2\mu \boldsymbol{e}^{\mathrm{e}} \tag{3}$$

where $\boldsymbol{\sigma}$ is the Cauchy stress, $\mathbb{C}^{\mathrm{e}}$ is the fourth-order elasticity tensor, κ is the bulk modulus, μ is the shear modulus, $\mathbf{1}$ is the second-order identity tensor, and $\boldsymbol{I}^{\mathrm{dev}}$ is the fourth-order transformation tensor that maps a second-order tensor to its deviatoric components. Also, $\epsilon^{\mathrm{e}}_{\mathrm{v}} = \mathrm{tr}\boldsymbol{\varepsilon}^{\mathrm{e}}$ and $\boldsymbol{e}^{\mathrm{e}}$ are the volumetric and deviatoric parts of the elastic strain, respectively, and the stress can be decomposed into the hydraulic pressure stress (mean stress) $\boldsymbol{\sigma}^{\mathrm{m}} = \frac{1}{3}(\mathrm{tr}\boldsymbol{\sigma})\mathbf{1}$ and the deviatoric stress $\boldsymbol{s} = \boldsymbol{\sigma} - \boldsymbol{\sigma}^{\mathrm{m}}$.

2.2.3. Isotropic elastoplastic constitutive law

The rate-independent inelastic behavior of the resin under consideration can be represented by the classical associative plasticity that assumes the von Mises yield criterion along with the isotropic non-linear hardening law. That is, we employ the following yield condition and hardening function:

$$f(\boldsymbol{\sigma}, \alpha_{\mathrm{p}}) = \|\boldsymbol{s}\| - \sqrt{\frac{2}{3}}\sigma_{\mathrm{y}}(\alpha_{\mathrm{p}}) = 0 \tag{4}$$

$$\sigma_{\mathrm{y}}(\alpha_{\mathrm{p}}) = \sigma_{\mathrm{y0}} + H\alpha_{\mathrm{p}} + R_0(1 - \exp(-\beta\alpha_{\mathrm{p}})) \tag{5}$$

where σ_{y0} is the initial yield stress, H, R_0, and β are the material parameters for the strain hardening. Here, the internal variable α_p is the accumulated plastic strain, which is defined as the time-integrated value of the following equivalent plastic strain rate:

$$\dot{\alpha}_p \equiv \dot{\bar{e}}^p = \sqrt{\frac{2}{3}}\|\dot{\boldsymbol{e}}^p\| \tag{6}$$

The flow rule, hardening rule, loading–unloading condition, and the consistency condition are, respectively, given as follows:

$$\dot{\boldsymbol{e}}^p = \dot{\gamma}_p \boldsymbol{N} \tag{7}$$

$$\dot{\alpha}_p = \sqrt{\frac{2}{3}}\dot{\gamma}_p \tag{8}$$

$$f(\boldsymbol{\sigma}, \alpha_p) \leq 0 \quad \dot{\gamma}_p \geq 0 \quad \dot{\gamma}_p f(\boldsymbol{\sigma}, \alpha_p) = 0 \tag{9}$$

$$\dot{\gamma}_p \dot{f}(\boldsymbol{\sigma}, \alpha_p) = 0 \tag{10}$$

where $\boldsymbol{N} = \partial f / \partial \boldsymbol{\sigma} = \boldsymbol{s}/\|\boldsymbol{s}\|$ is the flow vector, which is an effective second-order tensor that postulates the flow direction, and $\dot{\gamma}_p$ is the plastic multiplier, which is a non-negative scalar variable.

2.2.4. Isotropic creep model

The rate-dependent inelastic deformation is also considered for the resin in this study and can be realized by the creep strain $\boldsymbol{\varepsilon}^c$. Then, we assume that the rate of the creep strain $\underline{\boldsymbol{e}}^c$ follows the flow rule with the same flow vector $\boldsymbol{N}$ in (7) as

$$\underline{\boldsymbol{e}}^c = \dot{\gamma}_c \boldsymbol{N} \tag{11}$$

Defining the equivalent creep strain rate $\dot{\alpha}_c \equiv \dot{\bar{e}}^c$ similar to the definition of the equivalent plastic strain (6), we assume the following functional form for its evolution:

$$\dot{\bar{e}}^c = C_1(\bar{\sigma})^{C_2} \exp\left(-\frac{C_3}{T}\right) t^{C_4} \tag{12}$$

$$\dot{\alpha}_c = \sqrt{\frac{2}{3}}\dot{\gamma}_c \tag{13}$$

where C_1, C_2, C_3, and C_4 are the material parameters. Here, $\bar{\sigma} = \sqrt{\frac{3}{2}\boldsymbol{s}:\boldsymbol{s}} = \sqrt{\frac{3}{2}}\|\boldsymbol{s}\|$ is the von Mises equivalent stress, T is the absolute temperature, and t is the time. Since the parameters C_3 and C_1 are not independent, we fixed the latter parameter at $C_1 = 1.0$ assuming room temperature environments in this paper. For the sake of simplicity, the time-hardening term is also neglected, implying that $C_4 = 0$ is assumed.

2.2.5. Isotropic damage model

In order to represent the reduction of the elastic modulus, which is pointed out in the previous section as feature (d), we employ the damage variable that is a function of the

deformation history. More specifically, the elastic modulus in (3) is assumed to vary according to the following form:

$$E = (1 - D)E_0 \tag{14}$$

where E is the reduced elastic modulus by the active damage variable $0 < D < 1$. Here, E_0 is the elastic modulus of the virgin state of the material. In this study, we assume that the damage parameter evolves according to the following simple functional form:

$$D(\bar{\varepsilon}) = d_1(\bar{\varepsilon}_{\max})^{d_2} \quad 0 \leq D < 1 \tag{15}$$

where d_1 and d_2 are the material parameters, $\bar{\varepsilon}_{\max}$ is the maximum equivalent strain that the material ever experienced. In this study, a simple measure is assumed for the equivalent strain as $\bar{\varepsilon} = \sqrt{\frac{2}{3}\boldsymbol{e} : \boldsymbol{e}}$. Then, the maximum value is updated as $\bar{\varepsilon}_{\max} = \bar{\varepsilon}$, if and only if $\bar{\varepsilon} > \bar{\varepsilon}_{\max}$ is satisfied.

2.2.6. Combined model

All the constitutive equations introduced above are unified into the isotropic elastoplastic-creep-damage model for the polycarbonate resin in CFRP.

The elastic strain required to evaluate the stress can be represented as $\boldsymbol{\varepsilon}^{\mathrm{e}} = \boldsymbol{\varepsilon} - \boldsymbol{e}^{\mathrm{p}} - \boldsymbol{e}^{\mathrm{c}}$ in view of (2), but the plastic and creep strains are obtained by the time integration of the corresponding rates whose evolutions are postulated by the flow rules (7) and (11), respectively. Since the implicit algorithm is employed for the time integration, these inelastic strain rates (or increments) are determined by solving the system of return mapping equations for multipliers $\dot{\gamma}_{\mathrm{p}}$ and $\dot{\gamma}_{\mathrm{c}}$. Therefore, the amount or share of each strain can be determined as a result of their mutual interaction. On the other hand, since the material is assumed to suffer internal damage such that the 'elastic' modulus is reduced according to the maximum strain ever experienced, the effects of the inelastic strains on the damage parameter are indirect through the additive decomposition (2).

There must be room for argument on the employed material models, as they are somewhat crude. However, they are considered to be enough for the purpose of this study, since we are concerned with neither the development of new constitutive laws nor the employment or improvement of more sophisticated models.

3. NMT

In this section, the NMTs are conducted to characterize the macro- and microscopic material behavior of unidirectional CFRP, composed of polycarbonate resin and fibers. The method proposed in [40] is adopted for the FE analyses for the NMT, which we carry out with a general-purpose FEM software, ANSYS.[44] In preparation for the NMT, we perform the parameter identification for the isotropic elastoplastic-creep-damage combined model that is presented in the previous section, and investigate the evolutions of inelastic deformations evaluated with the constitutive model.

3.1. *Identification of material parameters*

This section is devoted to the identification of the material parameters in the constitutive model employed for the polycarbonate resin of CFRP. That is, using the test data

obtained in Section 2.1, we identify the material parameters used in the isotropic elastoplastic-creep-damage combined constitutive model introduced in the previous section. The method of particle swarm optimization (PSO),[42,43] which is one of the population-based descent methods, is employed for the identification algorithm.

Prior to the application of PSO, we first determine the elastic modulus as 2.5 (GPa) directly from the stress–strain curves in Figure 1, noting that the initial inclinations of the two curves are identical. Since the transverse deformations or Poisson's effects have not been measured in the experiments, the one-dimensional version of the employed constitutive model is used for the identification with the Poisson's ratio being fixed at 0.3 for three-dimensional cases.

Table 1 presents the identified values of material parameters and Figure 2 shows the stress–strain curves determined by those values along with the test data. As can be seen from these results, the identification seems to be successful, since each identified curve qualitatively reproduces the corresponding empirical ones. In fact, all of the features (a), (b), (c), and (d) pointed out in Section 2.1 are observed in the identified curves; that is, (b) the faster the strain rate, the higher the apparent stiffness, (c) the faster the strain rate, the smaller the residual deformation, and (d) the elastic modulus during the unloading regime is smaller than that of the loading regime.

3.2. *Time variation of internal variables*

In this section, we present the features of the combined constitutive model employed in this study by investigating the histories of some internal variables during the deformation process corresponding to Figure 2.

Figure 3 shows the variation of damage variable D with respect to the total strain. Since we assume that the internal damage depends only on the total strain, the variation does not depend on the deformation rate; that is, the curves with different strain rates are identical.

Figure 4 shows the time variation of plastic and creep strains with respect to the total strain. In the slower case with strain rate $0.0001/\mathrm{s}$, the plastic and creep strains vary with time on almost the same degree. On the other hand, in the faster case with strain rate $0.001/\mathrm{s}$, the amount of plastic strain becomes larger than that of creep strain. That is, as the strain rate is high, the share of the rate-dependent (creep) strain in the

Table 1. Identified values of material parameters.

Material parameters	Symbols	Identified values
Initial elastic modulus (MPa)	E	2500*
Initial yield stress (MPa)	σ_{y0}	39.40
Hardening parameters (MPa)	H	579.4
	R_0	26.57
	β	391.4
Creep parameter	C_2	3.223
	C_3	7249
Damage parameter	d_1	7.272
	d_2	0.9296

*Fixed value (not identified).

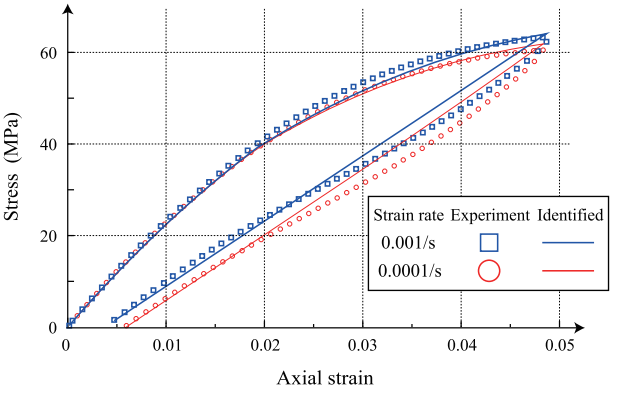

Figure 2. Stress–strain curves identified with PSO and test data.

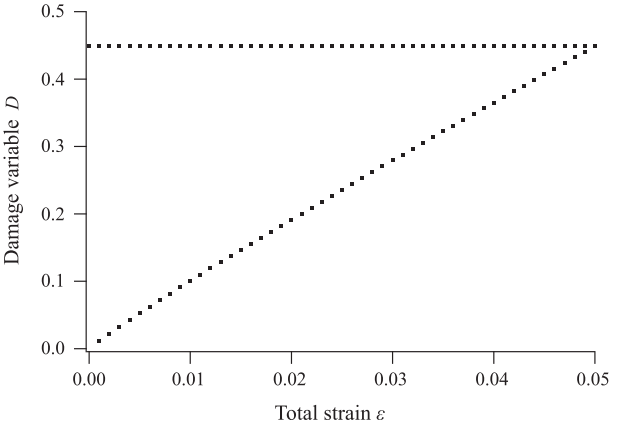

Figure 3. Variation of damage variable with respect to total strain.

total strain is reduced and at the same time the rate-independent (plastic) strain becomes dominant. These features are the manifestations of the discussion at the last part of Section 2.2 about the mutual interaction between plastic and creep strains.

Thus, the elastoplastic-creep-damage combined model introduced in this study enables us to reduce the degree of rate dependency as needed and, as an extreme case, to represent only the rate-independent deformation. However, the deficiencies of the model are pointed out especially when it is subjected to practical use. First of all, although it is empirically known that the resin material under consideration exhibits such a special rate dependency, it can hardly be confirmed only with the test data used for reference purpose. To validate the modeling, we have to prepare more reliable test data by conducting elaborate experiments. The second remark arises from the empirical fact that the residual deformation gradually diminishes after the external loading is released. The present model cannot reproduce such a time-dependent response. The third one is the lack of ability for representing the non-linearity of the unloading curve observed in Figure 1. This is partially due to the assumption that the elastic modulus

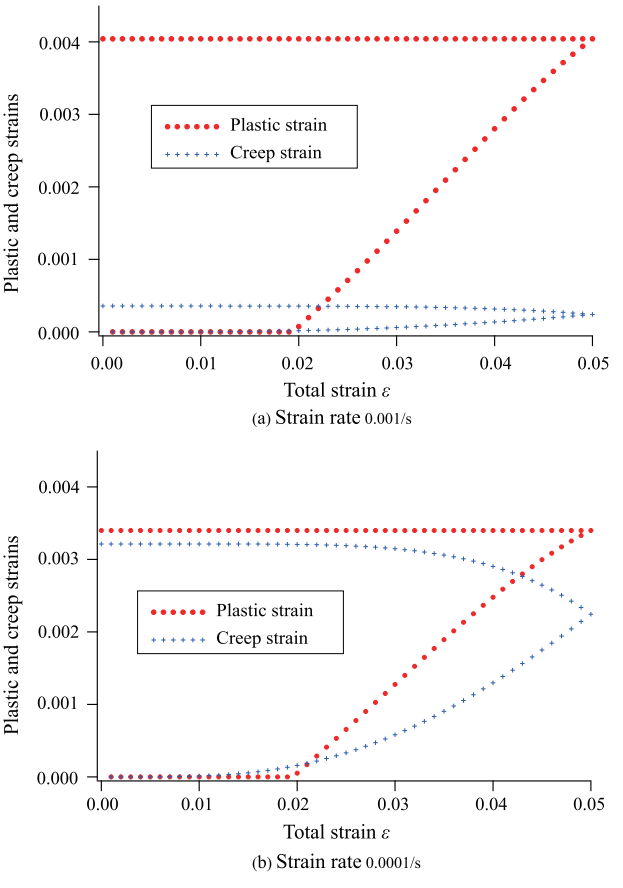

Figure 4. Variation of inelastic strains with respect to total strain.

remains constant during the loading. But, less importance is given to this behavior in this paper, as remarked in Section 2.1.

3.3. *Analytical model and conditions for NMT*

Figure 5 shows the prepared unit cell model of unidirectional CFRP, which is regarded as a 'specimen' for the NMT. The FE mesh is generated with 10-node tetrahedral elements. While we employ the combined model for the resin material with the identified values of the material parameters in the previous section, the nominal elastic properties (Young's modulus 230 GPa and Poisson's ratio 0.2) are used for the fibers.

In order to obtain the numerical test data of the macroscopic stress responses, we apply six basic patterns of macroscopic strains as loading parameters by imposing the relative displacements between periodic pairs of nodes on the external boundaries of the unit cell. This realizes the imposition of periodic boundary conditions for disturbance displacements associated with the micro-scale heterogeneity, which are induced by uniform deformations of the macroscopic strains; see e.g. [40].

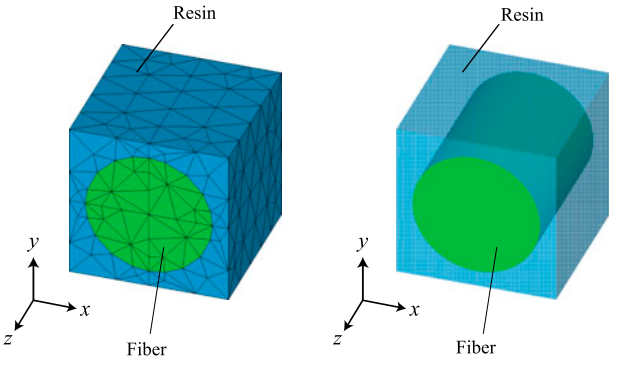

Figure 5. Unit cell model of unidirectional CFRP.

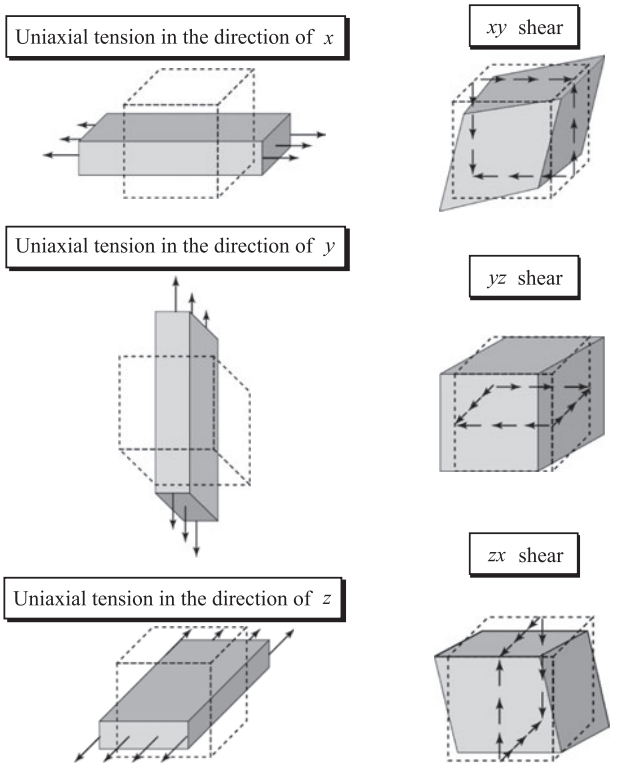

Figure 6. Deformation patterns for unit cell.

The six patterns of applied macroscopic deformations are depicted in Figure 6. Three of them are uniform normal strains without transverse and shear deformations, while the other three are simple shear stains without normal and transverse deformations. Two cases of strain rates are taken as in Section 3.1; that is, they are set at 0.0001/s and 0.001/s for both normal and shear strains. In each test case, the macroscopic strain component is gradually increased during the loading regime, until it

reaches the maximum 2.5%. The unloading is performed until the macroscopic stress becomes zero with the same deformation rate being kept.

3.4. Results of NMT

The macroscopic stress–strain curves obtained in the NMT were provided in Figure 7, which reveal anisotropy due to the micro-scale morphology. As can be seen from Figure 7(b), the responses in the *z*-direction are almost linear, though this is a natural consequence of the linearly elastic response of the fiber, which sustains much greater stress than the matrix. As a result, neither rate dependency nor damage response is observed. On the other hand, due to the inelastic and damage responses of the matrix phase, all the other macroscopic behavior exhibits non-linearity during the loading regime and reduction of elastic modulus during the unloading regime. In addition, they are a little rate-dependent, reflecting the effect of creep deformation. Because of the stress-sustaining ability of the fiber, the rate dependency of the resin, typified in Figure 2, is less manifested.

It is, therefore, reasonably concluded that macroscopic material behavior generally follows those assumed for a microstructure (unit cell), though an obvious difference is anisotropic in elastic and inelastic material behaviors.

4. Macroscopic constitutive law

The discussions about the NMT results in the previous section motivate us to incorporate the anisotropy into the elastoplastic-creep-damage combined model, which

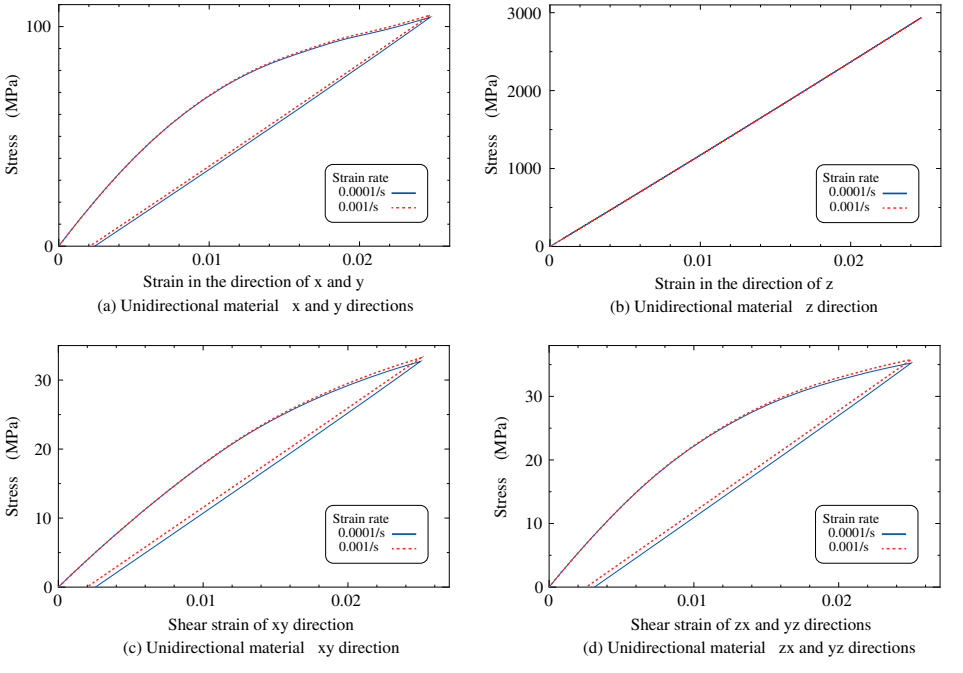

Figure 7. Results of numerical material tests for unidirectional CFRP.

is introduced in Section 2 for the polycarbonate resin, to represent the macroscopic material behavior of the unidirectional CFRP. In the following section, we first present the formulation of the proposed model for the CFRP, and then identify the material parameters by referring to the NMT results. With the identified parameters, the performance of the anisotropic model is demonstrated in terms of the analogy with the corresponding isotropic one that is used for the resin matrix.

4.1. *Anisotropic elastoplastic-creep-damage combined constitutive model*

In order to represent the macroscopic material behavior of the unidirectional CFRP, we propose an anisotropic elastoplastic-creep-damage combined model. Since micro- and macroscopic field variables are defined with respect to the micro- and macroscopic spatial coordinate systems, within the framework of the mathematical homogenization, they are commonly distinguished in the formulation with different symbols. In this context, the variables in Section 2 are microscopic ones, while those in this section are macroscopic ones. However, to avoid notational complexity, the same symbols are used for some of the macroscopic variables in this section. This is possible since the coupling between these variables can be realized only through the boundary conditions on unit cells; see Ref [40] for the detailed explanations.

4.1.1. *Orthotropic elastic constitutive model*

Orthotropy is assumed for the macroscopic elastic properties in view of extensibility, though transverse isotropy is sufficient for the present situation of the unidirectional CFRP. The corresponding generalized Hooke's law, which relates the stress and elastic strain tensors, $\boldsymbol{\sigma}$ and $\boldsymbol{\varepsilon}^{\mathrm{e}}$, is given as

$$\boldsymbol{\sigma} = \mathbb{C}_0^{\mathrm{e}} : \boldsymbol{\varepsilon}^{\mathrm{e}} \tag{16}$$

Here, as in Section 2, the elastic strain is defined as $\boldsymbol{\varepsilon}^{\mathrm{e}} \equiv \boldsymbol{\varepsilon} - \boldsymbol{\varepsilon}^{\mathrm{p}} - \boldsymbol{\varepsilon}^{\mathrm{c}}$ where $\boldsymbol{\varepsilon}$, $\boldsymbol{\varepsilon}^{\mathrm{p}}$, and $\boldsymbol{\varepsilon}^{\mathrm{c}}$ are the total, plastic, and creep strain tensors, respectively. Also, $\mathbb{C}_0^{\mathrm{e}}$ is the fourth-order elasticity tensor in the absence of damage, and the components of the compliance tensor, which is the inverse of $\mathbb{C}_0^{\mathrm{e}}$, are given as follows:

$$[\mathbb{S}_0^{\mathrm{e}}] = \begin{bmatrix} \frac{1}{E_{xx}} & -\frac{\nu_{xy}}{E_{xx}} & -\frac{\nu_{xz}}{E_{xx}} & 0 & 0 & 0 \\ -\frac{\nu_{yx}}{E_{yy}} & \frac{1}{E_{yy}} & -\frac{\nu_{yz}}{E_{yy}} & 0 & 0 & 0 \\ -\frac{\nu_{zx}}{E_{zz}} & -\frac{\nu_{zy}}{E_{zz}} & \frac{1}{E_{zz}} & 0 & 0 & 0 \\ 0 & 0 & 0 & \frac{1}{G_{xy}} & 0 & 0 \\ 0 & 0 & 0 & 0 & \frac{1}{G_{yz}} & 0 \\ 0 & 0 & 0 & 0 & 0 & \frac{1}{G_{zx}} \end{bmatrix} \tag{17}$$

where E_{xx}, E_{yy}, and E_{zz} are the elastic moduli in the directions indicated by the attached subscripts, and G_{xy}, G_{yz}, and G_{zx} are the shear elastic moduli along the planes indicated by the subscripts. Also, ν_{xy}, ν_{yz}, and ν_{zx} are the Poisson's ratios for orthotropic elasticity; for example, ν_{xy} is the absolute value of the normal strain in the y-direction with respect to the normal strain in the x-direction.

4.1.2. Hill's orthotropic elastoplastic constitutive law

To represent the anisotropic plastic responses of the CFRP, we employ the Hill's orthotropic model,[45] which assumes the yield function as

$$\phi_{\mathrm{p}}(\boldsymbol{\sigma}, \alpha_{\mathrm{p}}) = \frac{1}{2}(\sigma_{\mathrm{pHill}})^2 - \frac{1}{2}(\sigma_y(\alpha_{\mathrm{p}}))^2 \leq 0 \tag{18}$$

where α_{p} is the accumulated plastic strain defined later, and σ_{pHill} is the plastic Hill's stress defined as

$$\sigma_{\mathrm{pHill}} = \sqrt{\boldsymbol{\sigma} : \boldsymbol{M}_{\mathrm{p}} : \boldsymbol{\sigma}} \tag{19}$$

Here, $\sigma_y(\alpha_{\mathrm{p}})$ is the hardening function with independent variable α_{p} and is assumed to have the same function as (5). Also, $\boldsymbol{M}_{\mathrm{p}}$ is the plastic Hill tensor whose components are given in a matrix form as

$$[\boldsymbol{M}_{\mathrm{p}}] = \begin{bmatrix} Q_{\mathrm{p}} + R_{\mathrm{p}} & -R_{\mathrm{p}} & -Q_{\mathrm{p}} & 0 & 0 & 0 \\ -R_{\mathrm{p}} & R_{\mathrm{p}} + P_{\mathrm{p}} & -P_{\mathrm{p}} & 0 & 0 & 0 \\ -Q_{\mathrm{p}} & -P_{\mathrm{p}} & P_{\mathrm{p}} + Q_{\mathrm{p}} & 0 & 0 & 0 \\ 0 & 0 & 0 & 2N_{\mathrm{p}} & 0 & 0 \\ 0 & 0 & 0 & 0 & 2L_{\mathrm{p}} & 0 \\ 0 & 0 & 0 & 0 & 0 & 2M_{\mathrm{p}} \end{bmatrix} \tag{20}$$

where the components are defined as follows:

$$P_{\mathrm{p}} = \frac{1}{2}\left(\frac{1}{R_{yy}^2} + \frac{1}{R_{zz}^2} - \frac{1}{R_{xx}^2}\right), \quad L_{\mathrm{p}} = \frac{3}{2}\frac{1}{R_{yz}^2}$$

$$Q_{\mathrm{p}} = \frac{1}{2}\left(\frac{1}{R_{zz}^2} + \frac{1}{R_{xx}^2} - \frac{1}{R_{yy}^2}\right), \quad M_{\mathrm{p}} = \frac{3}{2}\frac{1}{R_{zx}^2} \tag{21}$$

$$R_{\mathrm{p}} = \frac{1}{2}\left(\frac{1}{R_{xx}^2} + \frac{1}{R_{yy}^2} - \frac{1}{R_{zz}^2}\right), \quad N_{\mathrm{p}} = \frac{3}{2}\frac{1}{R_{xy}^2}$$

Here, R_{xx}, R_{yy}, R_{zz}, R_{xy}, R_{yz}, and R_{zx} are referred to as the Hill's constants for the present Hill's orthotropic plasticity model, and are defined by means of the initial yield stresses $\sigma_{xx}^{\mathrm{Y}}, \sigma_{yy}^{\mathrm{Y}}, \cdots, \tau_{zx}^{\mathrm{Y}}$ as

$$R_{xx} = \frac{\sigma_{xx}^{\mathrm{Y}}}{\sigma_0^{\mathrm{Y}}} \quad , R_{yy} = \frac{\sigma_{yy}^{\mathrm{Y}}}{\sigma_0^{\mathrm{Y}}}, \quad R_{zz} = \frac{\sigma_{zz}^{\mathrm{Y}}}{\sigma_0^{\mathrm{Y}}} \tag{22}$$

$$R_{xy} = \sqrt{3}\frac{\tau_{xy}^{\mathrm{Y}}}{\sigma_0^{\mathrm{Y}}}, \quad R_{yz} = \sqrt{3}\frac{\tau_{yz}^{\mathrm{Y}}}{\sigma_0^{\mathrm{Y}}}, \quad R_{zx} = \sqrt{3}\frac{\tau_{zx}^{\mathrm{Y}}}{\sigma_0^{\mathrm{Y}}} \tag{23}$$

where σ_0^{Y} is the reference stress. In this study, the minimum value among all the yield stress values is taken as the reference.

Under the assumption of associative plasticity, the flow rule with the Hill's potential (18) is given by

$$\underline{\varepsilon}^{\mathrm{p}} = \dot{\gamma}_{\mathrm{p}} \boldsymbol{M}_{\mathrm{p}} : \boldsymbol{\sigma} \tag{24}$$

where $\dot{\gamma}_{\mathrm{p}}$ is the plastic multiplier. Also, postulating the equivalent plastic strain rate $\dot{\bar{\varepsilon}}^{\mathrm{p}}$ satisfies the equivalency

$$\sigma_{\mathrm{pHill}}\dot{\bar{\varepsilon}}^{\mathrm{p}} = \boldsymbol{\sigma} : \underline{\varepsilon}^{\mathrm{p}}, \tag{25}$$

we introduce the following hardening law as an evolution equation of the accumulated plastic strain α_{p}

$$\dot{\alpha}_{\mathrm{p}} \equiv \dot{\bar{\varepsilon}}^{\mathrm{p}} = \dot{\gamma}_{\mathrm{p}}\sigma_{\mathrm{pHill}} \tag{26}$$

The addition of the following loading–unloading conditions completes the Hill's anisotropic plasticity model:

$$\dot{\gamma}_{\mathrm{p}} \geq 0,\ \phi_{\mathrm{p}} \leq 0,\ \dot{\gamma}_{\mathrm{p}}\phi_{\mathrm{p}} = 0 \tag{27}$$

4.1.3. *Hill's orthotropic creep model*

In this study, the Hill's orthotropic model is diverted to represent the macroscopic creep behavior characterized in the previous section. That is, referring to the Hill's plasticity model presented above, we introduce the following creep Hill's stress, creep flow rule, and hardening law:

$$\sigma_{\mathrm{cHill}} = \sqrt{\boldsymbol{\sigma} : \boldsymbol{M}_{\mathrm{c}} : \boldsymbol{\sigma}} \tag{28}$$

$$\underline{\varepsilon}^{\mathrm{c}} = \dot{\gamma}_{\mathrm{c}}\boldsymbol{M}_{\mathrm{c}} : \boldsymbol{\sigma} \tag{29}$$

$$\dot{\alpha}_{\mathrm{c}} \equiv \dot{\bar{\varepsilon}}^{\mathrm{c}} = \dot{\gamma}_{\mathrm{c}}\sigma_{\mathrm{cHill}} \tag{30}$$

where $\dot{\bar{\varepsilon}}^{\mathrm{c}}$ is the equivalent creep strain rate and $\dot{\gamma}_{\mathrm{c}}$ is the creep multiplier, whose evolution equation is assumed to be almost the same functional form of (13) as

$$\dot{\bar{\varepsilon}}^{\mathrm{c}} = C_1(\sigma_{\mathrm{cHill}})^{C_2}\exp\left(-\frac{C_3}{T}\right) \tag{31}$$

Here, C_1, C_2, and C_3 are the creep parameters, T is the absolute temperature, and $\boldsymbol{M}_{\mathrm{c}}$ is the creep Hill tensor whose components are given in a matrix form as

$$\boldsymbol{M}_{\mathrm{c}} = \begin{bmatrix} Q_{\mathrm{c}}+R_{\mathrm{c}} & -R_{\mathrm{c}} & -Q_{\mathrm{c}} & 0 & 0 & 0 \\ -R_{\mathrm{c}} & R_{\mathrm{c}}+P_{\mathrm{c}} & -P_{\mathrm{c}} & 0 & 0 & 0 \\ -Q_{\mathrm{c}} & -P_{\mathrm{c}} & P_{\mathrm{c}}+Q_{\mathrm{c}} & 0 & 0 & 0 \\ 0 & 0 & 0 & 2N_{\mathrm{c}} & 0 & 0 \\ 0 & 0 & 0 & 0 & 2L_{\mathrm{c}} & 0 \\ 0 & 0 & 0 & 0 & 0 & 2M_{\mathrm{c}} \end{bmatrix} \tag{32}$$

The components here are defined as follows:

$$P_{\mathrm{c}} = \frac{1}{2}\left(\frac{1}{S_{yy}^2}+\frac{1}{S_{zz}^2}-\frac{1}{S_{xx}^2}\right), \quad L_{\mathrm{c}} = \frac{3}{2}\frac{1}{S_{yz}^2}$$

$$Q_{\mathrm{c}} = \frac{1}{2}\left(\frac{1}{S_{zz}^2}+\frac{1}{S_{xx}^2}-\frac{1}{S_{yy}^2}\right), \quad M_{\mathrm{c}} = \frac{3}{2}\frac{1}{S_{zx}^2} \tag{33}$$

$$R_{\mathrm{c}} = \frac{1}{2}\left(\frac{1}{S_{xx}^2} + \frac{1}{S_{yy}^2} - \frac{1}{S_{zz}^2}\right), \quad N_{\mathrm{c}} = \frac{3}{2}\frac{1}{S_{xy}^2}$$

Here, the Hill's constants for the Hill's orthotropic creep model, S_{xx}, S_{yy}, S_{zz}, S_{xy}, S_{yz}, and S_{zx}, must be different from those for the Hill's plasticity model, but the definitions have not been settled in the literature. In this study, we employ the minimum elastic and shear moduli as the reference values for normal and shear deformations, respectively. That is, the following definitions are introduced:

$$S_{xx} = \frac{E_{xx}}{E_{\min}}, \quad S_{yy} = \frac{E_{yy}}{E_{\min}}, \quad S_{zz} = \frac{E_{zz}}{E_{\min}} \tag{34}$$

$$S_{xy} = \frac{G_{xy}}{G_{\min}}, \quad S_{yz} = \frac{G_{yz}}{G_{\min}}, \quad S_{zx} = \frac{G_{zx}}{G_{\min}} \tag{35}$$

where

$$E_{\min} = \min(E_{xx}, E_{yy}, E_{zz}) \tag{36}$$

$$G_{\min} = \min(G_{xy}, G_{yz}, G_{zx}) \tag{37}$$

Although the validity of these definitions is hard to verify, the elastic modulus can be similar to the elastic limits, i.e. yield stresses, in the creep model, since they are equivalent to the stress values at the initial state without creep deformations.

4.1.4. *Anisotropic damage model*

It can be reasonably assumed that the macroscopic damage behavior resembles the microscopic one of the resin matrix in that the elastic modulus is reduced according to the maximum strain ever experienced. Thus, we present the anisotropic damage model below by diverting the one introduced in Section 2.2.5, although it is somewhat crude in considering the anisotropy.

The same functional form as in (15) is assumed for the damage variable D. Assuming that each of the nine elastic moduli in the orthotropic elasticity tensor $\mathbb{C}_0^{\mathrm{e}}$ has its own damage state, we introduce multipliers for the components C_{ij} defined as

$$s_i(D) = (1 - S_i D) \quad i = 1, 2, \cdots, 9 \tag{38}$$

where S_i is the damage coefficients for D. Thus, the damaged orthotropic elasticity matrix is determined according to the single damage variable along with the nine damage coefficients such that

$$[\mathbb{C}^{\mathrm{e}}(D)] = \begin{bmatrix} s_1 C_{11} & s_4 C_{12} & s_5 C_{13} & 0 & 0 & 0 \\ & s_2 C_{22} & s_6 C_{23} & 0 & 0 & 0 \\ & & s_3 C_{33} & 0 & 0 & 0 \\ & & & s_7 C_{44} & 0 & 0 \\ & & & & s_8 C_{55} & 0 \\ sym. & & & & & s_9 C_{66} \end{bmatrix} \tag{39}$$

4.2. Performance assessment of macroscopic constitutive law

In this section, the performance of the anisotropic elastoplastic-creep-damage combined model proposed above is verified. First, we identify the material parameters of the proposed macroscopic material model by applying the PSO as in Section 2 with the NMT results provided in Section 3 being the input data. Then, to confirm the validity of this constitutive model, the stress–strain curves with these identified parameters (referred to as identified curves) are compared with the NMT results.

4.2.1. Preparation

The macroscopic constitutive model has lots of parameters to be identified, say about 24. Also, easiness or difficulty in the identification is different from each other. It is, therefore, unwise to identify all the parameters uniformly and simultaneously in view of identification accuracy. Keeping this in mind, we exclude some parameters that can be easily identified with analytical or numerical schemes, and that can be fixed with assumed constraint conditions. The parameters excluded in the identification are explained here.

If both the fibers and matrix are assumed not to exhibit inelastic behavior, the macroscopic orthotropic elasticity tensor can be excluded from the design variables in the PSO. In fact, we can easily identify its components by conducting the NMTs, which is nothing but the standard linear homogenization analyses. Here, the homogenized elastic material is assumed to be orthotropic in this study, although the behavior of the xy-plane of the unit cell depicted in Figure 5 is not isotropic strictly.

Also, the initial yield stresses for x- and y-directions and those of yz- and zx-planes are the same, respectively. Therefore, we impose constraints beforehand such that $\sigma_{xx}^{\mathrm{Y}} = \sigma_{yy}^{\mathrm{Y}}$ and $\tau_{yz}^{\mathrm{Y}} = \tau_{zx}^{\mathrm{Y}}$. On the other hand, creep parameters C_1 and C_3 are dependent since only one level of temperature is considered in this study. Therefore, only C_3 is considered as an unknown parameter with $C_1 = 1.00$ being fixed. Also, since there is no damage during the loading in the z-direction as can be seen in Figure 7, we exclude the corresponding damage coefficient S_2 by setting it at a very small number.

4.2.2. Parameter identification by PSO

Under the above conditions, we apply the PSO to identify the material parameters of the proposed macroscopic constitutive equations. The NMT results obtained in Section 3, which are the relationships between the macroscopic stress and strains, are taken as test data for the identification. The following function is used to evaluate the identification errors with $\boldsymbol{p}$ being a vector that stores the parameters to be identified with the PSO:

$$\chi(\boldsymbol{p}) = \sum_{\alpha=1}^{n_{\mathrm{test}}} \frac{1}{n_{\mathrm{step}}^{[\alpha]}} \frac{1}{\|\boldsymbol{\sigma}_{\mathrm{ref}}^{[\alpha]}\|} \left(\sum_{i=1}^{n_{\mathrm{step}}^{[\alpha]}} \|\boldsymbol{\sigma}^{[i,\alpha]}(\boldsymbol{p}) - \hat{\boldsymbol{\sigma}}^{[i,\alpha]}\| \right) \tag{40}$$

where n_{test} is the number of macroscopic deformation patterns in the NMT (6 in this study) and $n_{\mathrm{step}}^{[\alpha]}$ is the number of loading steps for pattern α. Here, $\boldsymbol{\sigma}^{[i,\alpha]}(\boldsymbol{p})$. is the macroscopic stress tensor for test α that is evaluated at the i-th step with the assumed parameters $\boldsymbol{p}$, while $\hat{\boldsymbol{\sigma}}^{[i,\alpha]}$ is the corresponding stress tensor obtained in the NMT

conducted in Section 3. Also, $\boldsymbol{\sigma}_{\mathrm{ref}}^{[\alpha]}$ is the reference tensor to normalize the error for test α, and is assumed to be the macroscopic stress with the maximum square norm. In addition, the norm of second-order tensor $\boldsymbol{A}$. is defined as $\|\boldsymbol{A}\| \equiv \sqrt{\boldsymbol{A} : \boldsymbol{A}}$.

The identified values of the material parameters are provided in Table 2 and the identified curves with these values are shown in Figures 8 and 9, where the curves obtained in the NMT are depicted for comparison. As can be seen from the figures, the identified curves seem to be of good approximations to the NMT results for the unidirectional CFRP. Discrepancies acknowledged here can be resolved by the introduction of more reliable optimization schemes, but at the same time might mark the limitation of the reproducing performance of the proposed macroscopic constitutive model. This point may well be left to argue in another opportunity, since the agreement between the identified curves and those of the NMTs seem to be satisfactory from practical points of view.

Figures 10 and 11 show the variations of the accumulated plastic strains evaluated by means of the proposed macroscopic constitutive equations with the identified parameters with respect to the macroscopic axial and shear strains. More specifically, Figure 10 presents the evolutions of the macroscopic accumulated plastic strains when all the NMT patterns of the macroscopic strain components are separately used to evaluate the proposed macroscopic model at the deformation rate $10^{-4}/\mathrm{s}$. Note here that the increase of the accumulated plastic strains in response to the macroscopic normal x- and y-directions becomes gentle during the loading regime. The reason is that the elastic modulus is gradually reduced due to the damage evolution and, as a result, the

Table 2. Identified values of macroscopic material parameters.

Material parameters	Symbols & identified values	
Young's modulus for x- and y-directions [MPa]	$E_{xx} = E_{yy}$	9048*
Young's modulus for z-direction [MPa]	E_{zz}	116,300*
Shear modulus for xy-plane [MPa]	G_{xy}	2023*
Shear modulus for yz- and zx-planes [MPa]	$G_{yz} = G_{zx}$	2797*
Poisson's ratio for x–y-directions	ν_{xy}	0.3106*
Poisson's ratios for y–z and z–x-directions	$\nu_{yz} = \nu_{zx}$	0.2021*
Initial yield stresses for x- and y-directions [MPa]	$\sigma_{xx}^{\mathrm{Y}} = \sigma_{yy}^{\mathrm{Y}}$	63.13
Initial yield stress for z-direction [MPa]	σ_{zz}^{Y}	2851
Initial yield stress for xy-plane [MPa]	τ_{xy}^{Y}	24.78
Initial yield stresses for yz- and zx-planes [MPa]	$\tau_{yz}^{\mathrm{Y}} = \tau_{zx}^{\mathrm{Y}}$	23.22
Hardening parameter 1 [MPa]	H	923.1
Hardening parameter 2 [MPa]	R_0	95.12
Hardening parameter 3	β	504.8
Creep parameter 1	C_1	1.000**
Creep parameter 2	C_2	1.165
Creep parameter 3	C_3	5034
Damage parameter 1	d_1	0.5976
Damage parameter 2	d_2	0.7428
Damage coefficient 1	S_1	14.71
Damage coefficient 2	S_2	10^{-10}**
Damage coefficient 3	S_3	5.152
Damage coefficient 4	S_4	29.45
Damage coefficient 5	S_5	12.78
Damage coefficient 6	S_6	15.65

*Evaluated with linear homogenization analysis.
**Fixed value (not identified).

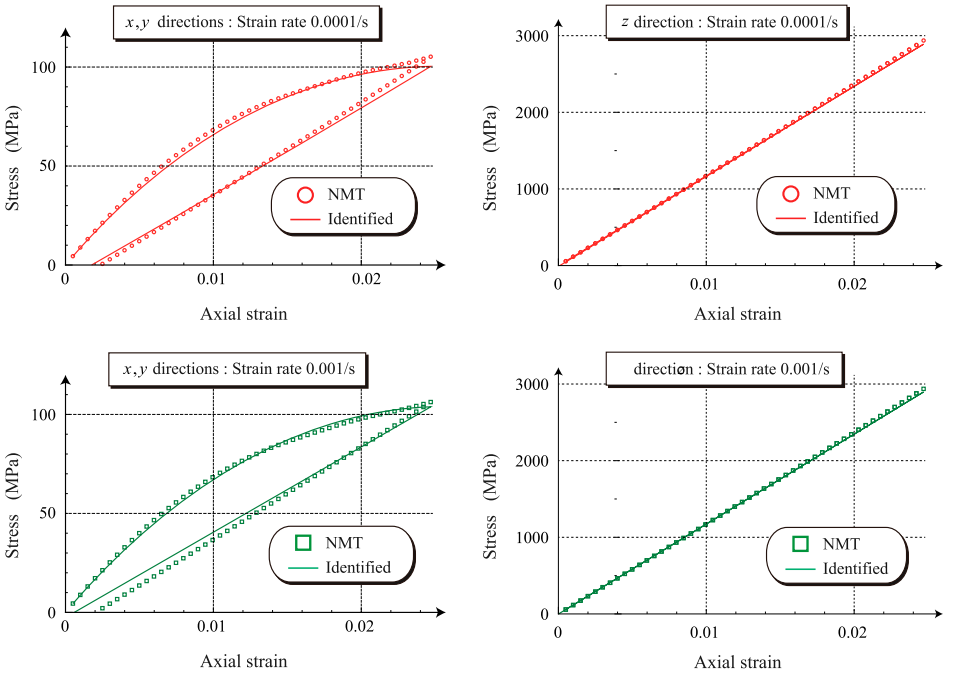

Figure 8. Identified curves with NMT results for unidirectional CFRP (axial and transverse directions).

increase of the plastic Hill's stress becomes gentle. Also, the accumulated plastic strain in response to the macroscopic normal strain in the z-direction is very small, since the fibers, which sustain much higher stresses than the matrix, are assumed not to exhibit inelastic deformations. On the other hand, Figure 11 shows the evolutions of the macroscopic accumulated creep strains when the proposed macroscopic model is evaluated separately with all the NMT patterns of the macroscopic strain components at a deformation rate $10^{-4}/\mathrm{s}$.

It is interesting to note that the accumulated plastic strains depicted in Figure 10 become large when the macroscopic shear deformations are imposed. But, the accumulated creep strains depicted in Figure 11 show the opposite trend. That is, the macroscopic normal strains tend to induce large amounts of the accumulated creep strains than the macroscopic shear strains do. This tendency is due to the fact that, with the present macroscopic constitutive model equipped with (31), the larger the creep strain, the higher the creep Hill's stress σ_{cHill}, and that macroscopic normal strains induce higher stresses than macroscopic shear strains in the case of unidirectional CFRP. On the other hand, the amount of plastic strain is determined according to not only the plastic Hill's stress, but also the assumed values of yield stresses and hardening characteristics. These are the functional features of the proposed model, which are inherited from the isotropic model used for the polycarbonate resin.

It follows from these discussions that the most important process of the two-scale analysis based on the homogenization is to introduce appropriate material models of

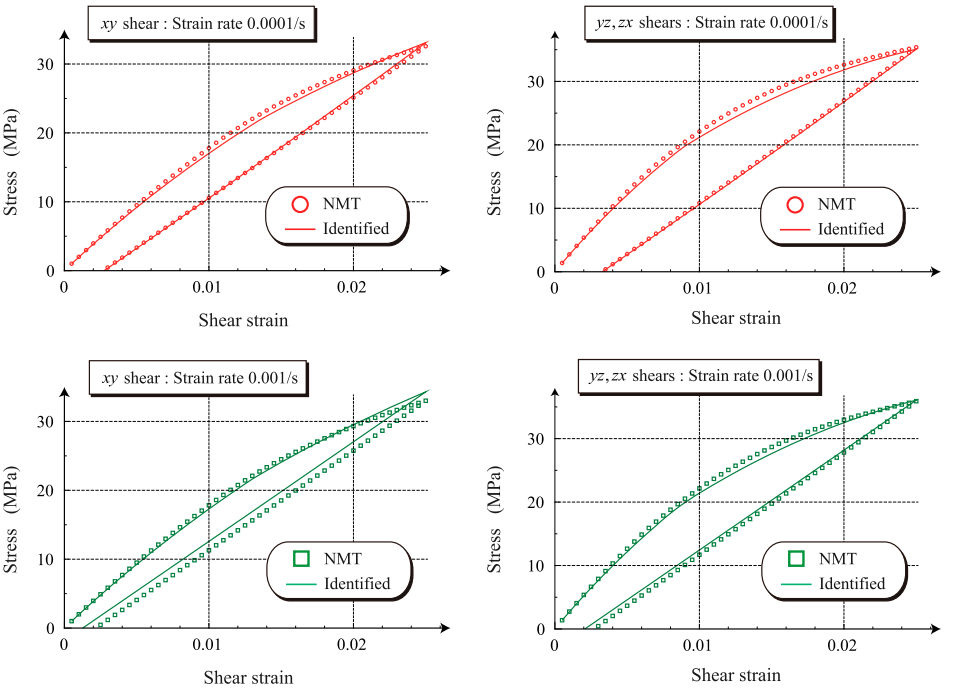

Figure 9. Identified curves with NMT results for unidirectional CFRP (shear directions).

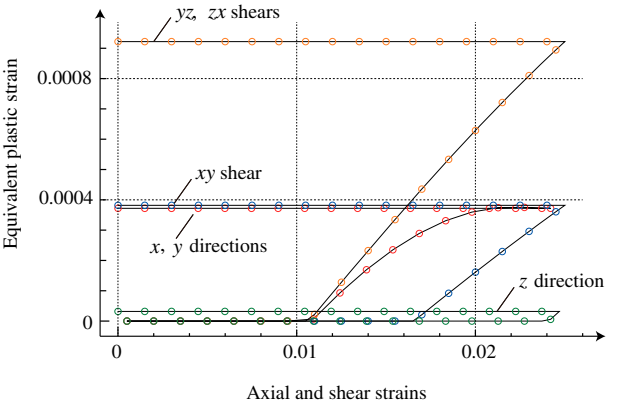

Figure 10. Evolutions of macroscopic accumulated plastic strains evaluated with identified parameters (strain rate: $10^{-4}/\mathrm{s}$).

constituents in a unit cell. This remark is applicable to both coupling and decoupling schemes, since material models in a unit cell are common. In conclusion, even if the identification errors for macroscopic material parameters are considered, the decoupling scheme has a higher utility value than the coupling one from practical viewpoints in that the former requires much less computational cost than the latter. It might be,

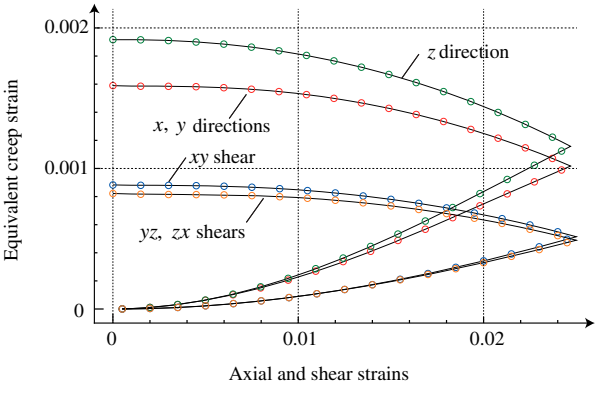

Figure 11. Evolutions of macroscopic accumulated creep strains evaluated with identified parameters (strain rate: 10^{-4}/s).

however, true that this conclusion applies mainly to the case such that the combination of constituents is simple as FRPs.

5. Macroscopic analysis and localization analysis

To demonstrate the capability of the method of decoupling two-scale analyses, we carry out the macroscopic analysis using the proposed macroscopic constitutive model with the material parameters identified in the previous section. Also, the macroscopic analysis is followed by the localization analysis, which enables us to reproduce the microscopic responses of the unit cell, located at a macroscopic material point of interest, during the macroscopic deformation process.

5.1. Analytical conditions

The FE model of the macrostructure of CFRP under consideration in the two-scale analysis is depicted in Figure 12 along with the constrained and loading conditions. This FE model consists of 10,000 twenty-node hexahedral elements and the total number of nodes is 32,149. As indicated in this figure, the fibers are assumed to be oriented in the direction inclined counterclockwise by 30° with respect to the x-axis. The FE analysis for this macroscopic model is conducted with ANSYS,[44] into which the proposed anisotropic elastoplastic-creep-damage combined model is installed as a user-material subroutine.

All the degrees of freedom of the nodes located on the upper and lower surfaces of the red frame indicated in Figure 12 are fixed at zero throughout the FE analysis. On the other hand, the displacement in the x_1-direction is enforced on all the nodes on the upper and lower surfaces of the yellow frame, while their degrees of freedom in the y- and z-directions are not constrained. The maximum value of the enforced displacement is 1.5% of gage length 109.3 mm, which is actually the total length of the specimen excluding the chuck lengths.

For the displacement control FE analysis, we prepare three levels of deformation rates, 'Fast,' 'Moderate,' and 'Slow,' each of which is set so that the total time needed for all the deformation processes is 12, 120, or 1200 s, respectively. The enforced

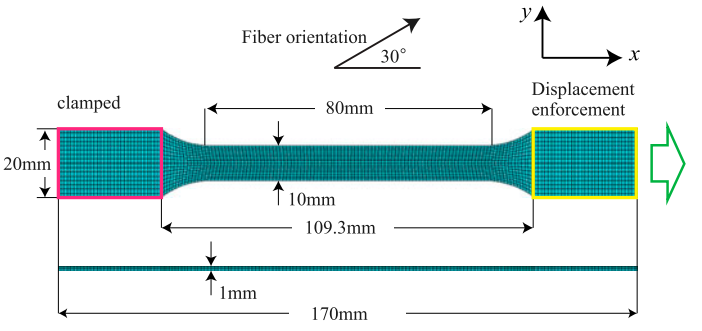

Figure 12. Finite element model of CFRP specimen.

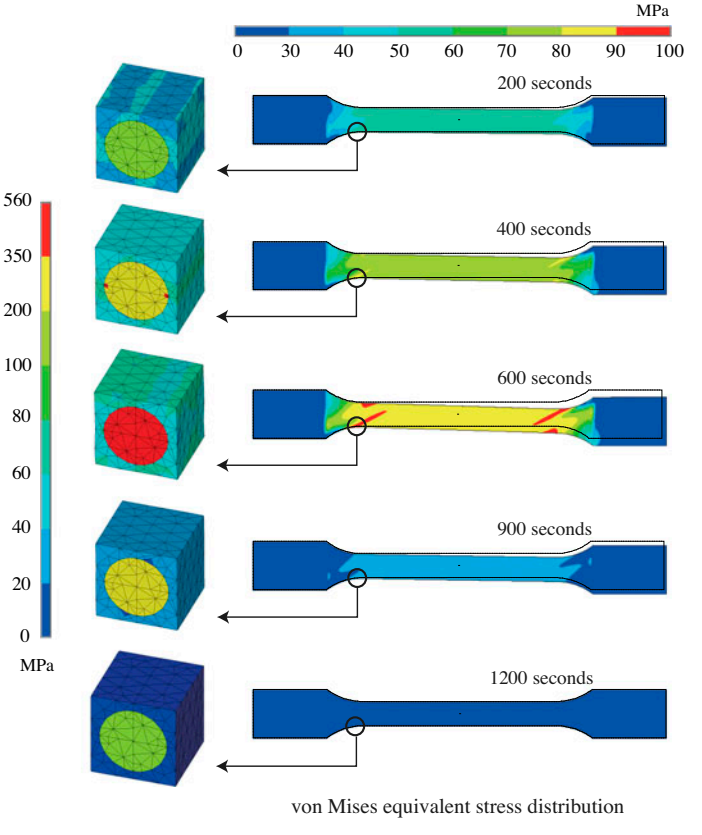

Figure 13. Results of macroscopic and localization analyses (von Mises equivalent stress distributions).

displacement is changed at each deformation rate and linearly with respect to real time during both the loading and unloading regimes.

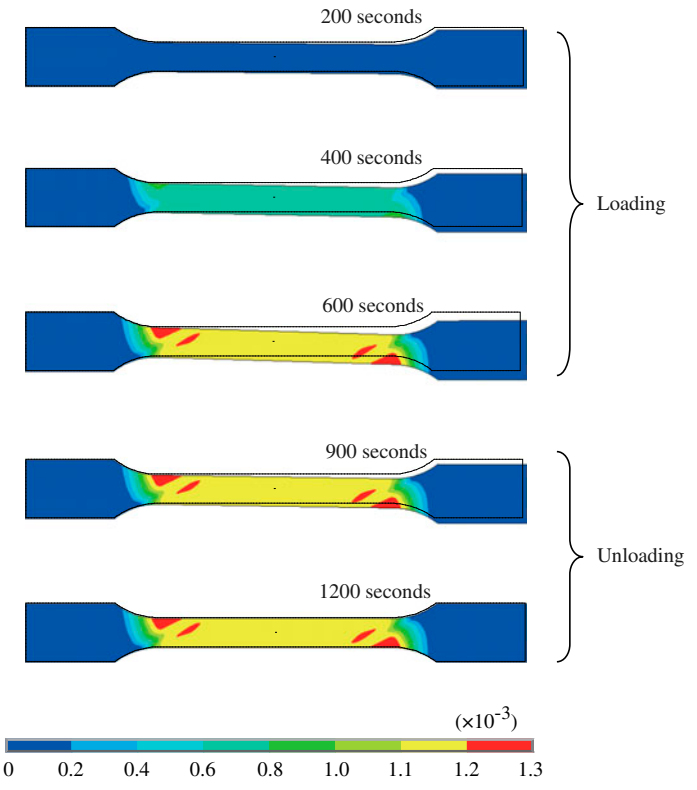

Figure 14. Results of macroscopic analysis (accumulated plastic strain distributions).

5.2. *Analysis result*

The result for 'Slow' case is given on the right-hand side of Figure 13, which shows the distributions of macroscopic von Mises stress along with the deformed configurations. Due to the orthotropic material behavior, the transverse deformation is observed in spite of the axial loading. Also, the stresses are concentrated around the regions between the base of the measurement section and the chucks, and reflect the material axis defined by the fiber orientation.

In order to demonstrate the localization capability of the decoupling two-scale analysis method, we extract the macroscopic deformation history at the point where the maximum value of the macroscopic von Mises stress is observed and impose it to the unit cell model in Figure 5 by following the method of NMT presented in Ref [40]. The results of these microscopic analyses are shown on the left-hand side of Figure 13, which illustrate the distributions of microscopic von Mises stress. As can be seen from the figure, the microscopic stress responses well reflect the macroscopic deformation history.

Figures 14–16 show the time variations of the macroscopic accumulated plastic and creep strains and the macroscopic damage variable for 'Slow' case. As can be seen from the figures, they have almost the same tendencies; that is, relatively large amounts of inelastic strains and damage variable are observed in the regions subjected to

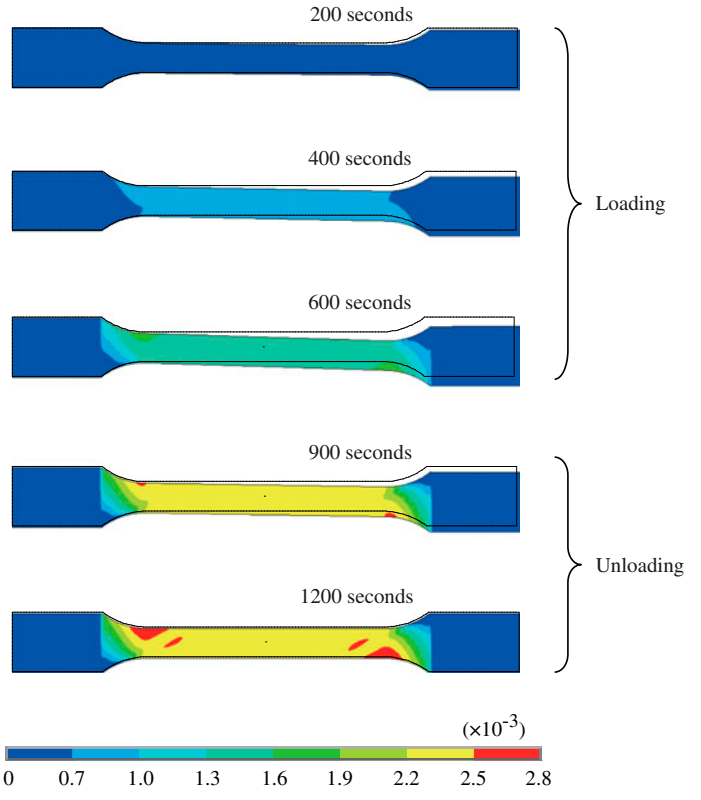

Figure 15. Results of macroscopic analysis (accumulated creep strain distributions).

macroscopically shear deformation. These are indeed typical of this type of orthotropic materials.

Figure 17 shows the relationships between the enforced displacements and the resultant forces in the loading direction that are the sums of the reaction forces evaluated at the constrained nodes on the chucks. As can be seen from the figure, the difference between the results of 'Fast' and 'Moderate' cases is small, while 'Slow' case typifies the effect of rate dependency. These are due to the fact that the faster the macroscopic deformation rate, the more dominant the plastic deformation in comparison with the creep deformation and that the slower the macroscopic deformation rate, the more dominant the creep deformation that is rate-dependent.

Let us examine further the shares of inelastic deformations that illustrate the points of the above discussion about the macroscopic material responses at different deformation rates, which are reasonably represented by the proposed constitutive model. Figures 18 and 19 show the evolutions of the accumulated plastic and creep strains evaluated at the point used for the localization analysis. It should be noted that the vertical axis of the latter graph is logarithmic scale. It can be seen from the figure that the plastic deformation is dominant and the creep deformation becomes very small throughout the FE analysis of 'Fast' case. This implies that the rate dependency is hard to appear when the macroscopic deformation rate is very high, and vice versa. Also, Figure 18 indicates that there is no evolution of plastic

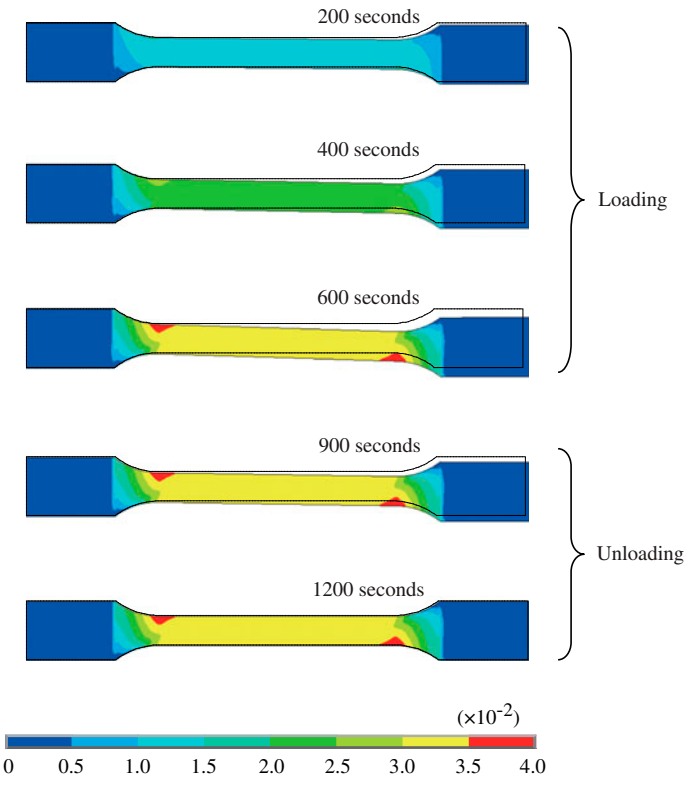

Figure 16. Results of macroscopic analysis (damage variable distributions).

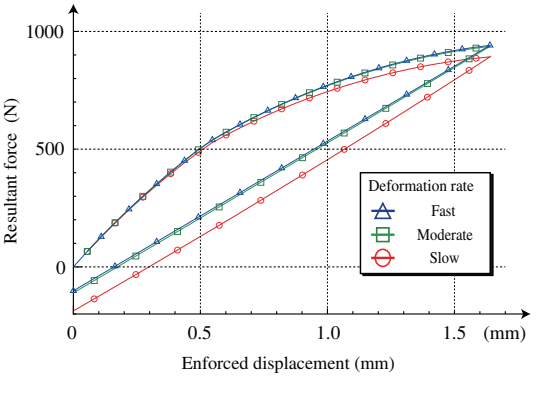

Figure 17. Results of macroscopic analysis (reaction force vs. enforced displacement).

strain during the unloading process, while the creep strain slightly increases even during the unloading process as illustrated in Figure 19. These features of the macroscopic constitutive model are also that of the microscopic ones for the resin matrix that are typified in Figures 14 and 15, respectively.

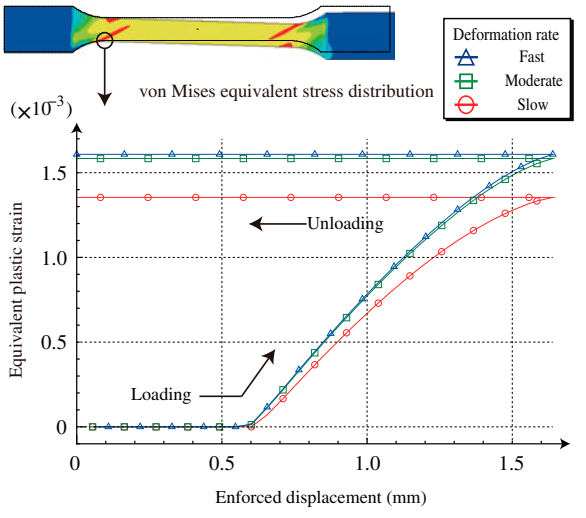

Figure 18. Results of macroscopic analysis (evolution of accumulated plastic strains).

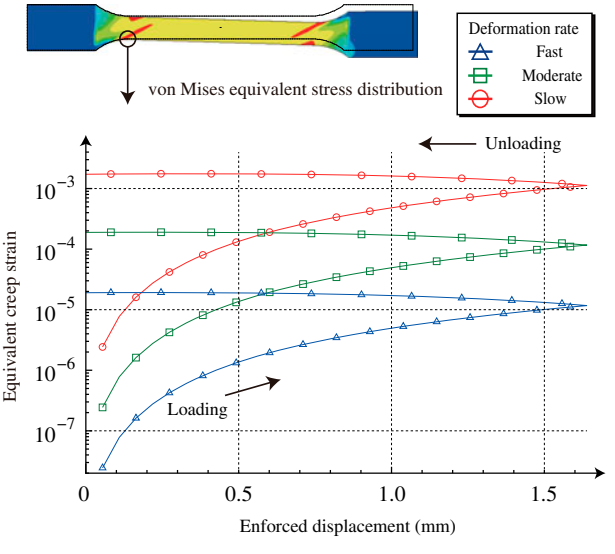

Figure 19. Results of macroscopic analysis (evolution of accumulated creep strains).

6. Conclusions

This study has been devoted to the illustration to confirm that the homogenization-based decoupling two-scale analyses are possible, even though relatively complex material behavior involving plastic-creep coupled deformations and internal damage is assumed for unit cells. It followed from the illustration that the accuracy of decoupling two-scale analyses was guaranteed to some degree, if appropriate macroscopic constitutive models could be formulated so as to inherit the features of the microscopic ones

introduced to unit cells. The concrete results have been achieved on the premise that the decoupling two-scale analyses would be applied to characterize the non-linear mechanical behavior of CFRP, which has relatively simple combination of constituents, and are itemized as follows:

- An isotropic elastoplastic-creep-damage combined constitutive model was introduced to characterize the inelastic material behavior of the polycarbonate resin commonly used in CFRP with reference to the actual test data.
- With the constitutive model along with the identified material parameters, a series of NMT was conducted to derive the macroscopic material responses.
- Referring to the NMT results and inheriting the features of the constitutive model for the resin, we proposed an anisotropic elastoplastic-creep-damage combined constitutive model to represent the macroscopic material behavior of CFRP. The proposed model is just a direct extension of the isotropic counterpart and is constructed as the combination of the existing anisotropic inelasticity models.
- By means of the PSO, we identified the material parameters of the proposed anisotropic constitutive model with reference to the NMT results. With the identified curves being compared with the NMT results, the accuracy of identification was qualitatively confirmed. At the same time, the macroscopic material behavior represented by the proposed constitutive model was studied in view of the analogy with the isotropic counterpart assumed for the microscopic material behavior.
- Using the proposed macroscopic constitutive model along with the identified material parameters, we presented a numerical example of the decoupling two-scale analysis. The macroscopic analysis is conducted on the specimen model, which was assumed to be made of CFRP, and was followed by the microscopic analysis to demonstrate the localization capability within the framework of homogenization theory. Paying attention to a single macroscopic material point, we examined the evolutions and shares of plastic and creep strains, and damage variables during the loading and unloading processes at different macroscopic deformation rates.

The important aspect of this study presupposes the use of the decoupling scheme that is superior to the coupling one in view of practical use for CAE. In fact, the authors have applied their efforts to promote the method of decoupling two-scale analysis based on homogenization theory by implementing the method of NMT along with identification functions and by installing the integrated environment for the micro- and macroscopic analyses into the general-purpose FEM software.[40,46] It is conceded that the results of this study are also eligible for the promotion.

However, the decoupling scheme is just an approximate scheme, since assumed macroscopic constitutive models do not always properly represent the macroscopic material behavior. Thus, two-scale analyses are responsible for the degree of approximation, and the coupling scheme can be used rather than the decoupling one, if the highest level of accuracy is desired irrespective of computational costs. Also, since large deformations of resin matrix have to be considered for design of FRP, the methodology presented in this study must be verified within the framework of finite strain theory. These issues and some others are to be addressed in the future.

References

[1] Hashin Z, Rosen BW. The elastic moduli of fiber-reinforced materials. J. Appl. Mech. 1964;31:223–232.
[2] Budiansky B. On the elastic moduli of some heterogeneous materials. J. Mech. Phys. Solids 1965;13:223–227.
[3] Hill R. A self-consistent mechanics of composite materials. J. Mech. Phys. Solids. 1965;13:213–222.
[4] Mori T, Tanaka K. Average stress in matrix and average elastic energy of materials with misfitting inclusions. Acta Metall. 1973;21:571–574.
[5] Hashin Z. Analysis of composite materials – a survey. J. Appl. Mech. 1983;50:481–505.
[6] Halpin JC. Primer on composite materials analysis. 2nd ed. Lancaster: Technomic Pub. Co.; 1984.
[7] Christensen RM. Mechanics of composite materials. New York (NY): Wiley; 1979.
[8] Mura T. Micromechanics of defects in solids. AA Dordrecht: Kluwer Academic; 1987.
[9] Chou T-W. Microstructural design of fiber composites. Cambridge: Cambridge University Press; 1992.
[10] Nemat-Nasser S, Hori M. Micromechanics: overall properties of heterogeneous materials. Amsterdam: North-Holland; 1993.
[11] Reddy JN, Miravete A. Practical analysis of composite laminates. Boca Raton: CRC Press; 1995.
[12] Kaminski MM. Computational mechanics of composite materials: sensitivity, randomness and multiscale behaviour. Berlin: Springer; 2005.
[13] Zohdi TI, Wriggers P. An introduction to computational micromechanics. London: Springer; 2005.
[14] Mishnaevsky LL. Computational mesomechanics of composites: numerical analysis of the effect of microstructures of composites of strength and damage resistance. Chichester: John Wiley; 2007.
[15] Barbero EJ. Finite element analysis of composite materials. Boca Raton: CRC Press; 2007.
[16] Benssousan A, Lions J-L, Papanicoulau G. Asymptotic analysis for periodic structures. Amsterdam: North-Holland; 1978.
[17] Sanchez-Palencia E. Non-homogeneous media and vibration theory. Berlin: Springer-Verlag; 1080.
[18] Lions J-L. Some methods in mathematical analysis of systems and their control. Beijing: Kexue Chubanshe Science Press and Gordon & Breach Science Pub; 1981.
[19] Suquet PM. Elements of homogenization theory for inelastic solid mechanics. In: Sanchez-Palencia E, Zaoui A, editors. Homogenization techniques for composite media. Berlin: Springer-Verlag; 1987. p. 193–278.
[20] Konke C. Damage evolution in ductile materials: from micro- to macro-damage. Comput. Mech. 1995;15:497–510.
[21] Lee K, Moorthy S, Ghosh S. Multiple scale computational model for damage in composite materials. Comput. Methods Appl. Mech. Eng. 1999;172:175–201.
[22] Fish J, Yu Qing, Shek K. Computational damage mechanics for composite materials based on mathematical homogenization. Int. J. Numer. Methods Eng. 1999;45:1657–1679.
[23] Kondo K, Takiguchi R. Finite element analysis of creep in unidirectional composites based on homogenization theory. Adv. Compos. Mater. 2002;11:31–39.
[24] Nishikawa M, Okabe T, Takeda N. Periodic-cell simulations for the microscopic damage and strength properties of discontinuous carbon fiber-reinforced plastic composites. Adv. Compos. Mater. 2009;18:77–93.
[25] Yoshimura A, Okabe T. Damage growth analysis in particle-reinforced composite using cohesive element. Adv. Compos. Mater. 2011;20:569–583.
[26] Okabe T, Motani T, Nishikawa M, Hashimoto M. Numerical simulation of microscopic damage and strength of fiber-reinforced plastic composites. Adv. Compos. Mater. 2012;21:147–163.
[27] Terada K, Kikuchi N. Nonlinear homogenization method for practical applications. In: Ghosh S, Ostoja-Starzewski M, editors. Vol. AMD-212/MD-62. Computational methods in micromechanics. New York (NY): AMSE; 1995. p. 1–16.

[28] Smit RJM, Brekelmans WAM, Meijer HEH. Prediction of the mechanical behavior of nonlinear heterogeneous systems by multi-level finite element modeling. Comput. Methods Appl. Mech. Eng. 1998;155:181–192.
[29] Więckowski Z. Dual finite element methods in homogenization for elastic–plastic fibrous composite material. Int. J. Plast. 2000;16:199–221.
[30] Zheng SF, Ding K, Denda M, Weng GJ. A dual homogenization and finite-element study on the in-plane local and global behavior of a nonlinear coated fiber composite. Comput. Methods Appl. Mech. Eng. 2000;183:141–155.
[31] Feyel F, Chaboche JL. FE^2 multiscale approach for modelling the elastoviscoplastic behaviour of long fibre SiC/Ti composite materials. Comput. Methods Appl. Mech. Eng. 2000;183:309–330.
[32] Terada K, Kikuchi N. A class of general algorithms for multi-scale analyses of heterogeneous media. Comput. Methods Appl. Mech. Eng. 2001;190:5427–5464.
[33] Terada K, Saiki I, Matsui K, Yamakawa Y. Two-scale kinematics and linearization for simultaneous two-scale analysis of periodic heterogeneous solids at finite strain. Comput. Methods Appl. Mech. Eng. 2003;192:3531–3563.
[34] Kaneko K, Terada K, Kyoya T, Kishino Y. Global–local analysis of granular media in quasi-static equilibrium. Int. J. Solids Struct. 2003;40:4043–4069.
[35] Terada K, Kurumatani M. Two-scale diffusion-deformation coupling model for material deterioration involving micro-crack propagation. Int. J. Numer. Methods Eng. 2010;83:426–451.
[36] Yamada T. Iterative algorithms for computing the averaged response of nonlinear composites under stress-controlled loadings. Int. J. Multiscale Comput. Eng. 2006;4:475–486.
[37] Temizer İ, Wriggers P. An adaptive method for homogenization in orthotropic nonlinear elasticity. Comput. Methods Appl. Mech. Eng. 2007;196:3409–3423.
[38] Matsui K, Terada K, Yuge K. Two-scale finite element analysis of heterogeneous solids with periodic microstructures. Comput. Struct. 2004;82:593–606.
[39] Watanabe I, Terada K. A method of predicting macroscopic yield strength of polycrystalline metals subjected to plastic forming by micro–macro de-coupling scheme. Int. J. Mech. Sci. 2010;52:343–355.
[40] Terada K, Kato J, Hirayama N, Inugai T, Yamamoto K. A method of two-scale analysis with micro–macro decoupling scheme: application to hyperelastic composite materials. Comput. Mech. 2013;52:1199–1219.
[41] Simo JC, Hughes TJR. Computational inelasticity, interdisciplinary applied mathematics. Vol. 7. New York (NY): Springer; 1998.
[42] Eberhart RC, Kennedy J. A new optimizer using particle swarm theory. Proceedings of the Sixth International Symposium on Micromachine and Human Science; 1995; Nagoya, Japan. p. 1–2.
[43] Kennedy J, Eberhart RC. Particle swarm optimization. Proceedings of IEEE the International Conference on Neural Networks; 1995; Piscataway, NJ. p. 1942–1948.
[44] ANSYS Inc. Release 13.0 Documentation for ANSYS; 2011.
[45] de Souza Neto EA, Peri D, Owen DRJ. Computational methods for plasticity. Singapore: Wiley; 2008.
[46] Cybernet Systems Co. Ltd. [cited 2013 Dec]. Available from: http://www.cybernet.co.jp/ansys/multiscale/multiscale_sim/